

Quantum-well states and discontinuities in opto-electrical characteristics of SCH lasers.

Z. Koziol*

Orel State Technical University,
29 Naugorskoye Shosse, Orel, 302020, Russia.

November 8, 2018

Abstract

Computer simulations with Synopsys' Sentaurus TCAD of opto-electrical characteristics of separate-confinement heterostructure laser based on *AlGaAs* are used as an example to study the role of the width and depth of Quantum Well (QW) active region on laser characteristics, I-V and I-L, below and above the lasing threshold. The device properties depend on both, the number of bound QW states and on closeness of the highest bound states to conduction or valence band offset. The lasing action may not exist at certain widths or heights of QW, the threshold current is a discontinuous function of these parameters. The effects are more pronounced at low temperatures. Discontinuities in characteristics may be observed at certain conditions in temperature dependencies of laser parameters.

1 Introduction

Computer modelling of electronic devices is a relatively new approach towards study of physical phenomena occurring there as well optimizing their

*Corresponding author email: zbigniew@ostu.ru

technical characteristics. Methodologically, this field of scientific and engineering activity may be placed between theory and experiment: pursuing research of that kind requires theoretical understanding of physics of microscopic processes and may work as a helpful tool in interpretation of experimental data. However, contrary to sometime met thinking, computer modelling can not replace either theory or experiment. But in some situations, results of that research may provide an inspiration for understanding or testing physical phenomena: it is easier, faster and less expensive to perform modelling than experiments, and we are not restricted that much by, often large, inaccuracy of experimental data that may hide insightful details.

When performing modelling *AlGaAs* SCH lasers with Synopsys' Sentaurus TCAD [1], we noticed unexpected steps in some of their characteristics (threshold current I_{th} versus the width of quantum well d_a , or versus its height, etc). Analyses of results led us to an idea that observed discontinuities occur when the most upper bound QW state crosses the conduction or valance band offset energy. Following that idea, we guessed that the effects may manifest itself in temperature dependence of some quantities as well, if laser parameters are chosen for that properly. The discontinuities are found also below the lasing threshold current, in their $I - V$ characteristics or in gain (or loss) versus current.

We attribute the existence of observed effects to tunneling transport phenomena through QW. When the dimensions of the structure are reduced below the mean free path (which is of the order of $10^2 - 10^4 \text{ nm}$ for AlGaAs), one enters the ballistic transport regime; drift-diffusion model of carriers transport must be replaced with transfer method type of calculations when dealing with QW widths of the order of 10nm [2].

2 Modelling

The laser we are modelling has dimensions, structure and doping as described by Andreev, et al. [3], [4]. The lasing wavelength is 808nm . The lasing offset voltage U_0 is $1.56 - 1.60\text{V}$, differential resistance just above the lasing offset, $r = dU/dI$ is $50 - 80\text{m}\Omega$, threshold current I_{th} is $200 - 300\text{mA}$, slope of optical power, $S = dL/dI$ is $1.15 - 1.25\text{W/A}$, and left and right mirror reflection coefficients R_l and R_r are 0.05 and 0.95. The reference laser has the width of QW, d_a , of 12nm and both waveguides' width is $0.2\mu\text{m}$. In order to reproduce laser characteristics in computational results, we played with several variables available in Synopsys. The critical one is A_{ph} - the effective surface area

Table 1: A few sets of simulation conditions ($A - F$) for data shown in Figures 2 and 4. C is radiative recombination rate (Eq. 2). α_n , and α_p are coefficients of free carrier absorption formula (1). Temperature for all cases is $T = 300K$, electron and hole scattering times are assumed $8 \cdot 10^{-13}s$ and $4 \cdot 10^{-13}s$, respectively, and electron and hole mobility $9200cm^2/Vs$ and $400cm^2/Vs$, respectively. No SRH recombination and no additional light scattering mechanisms are assumed.

#	$C [cm^3/s]$	$\alpha_n [cm^{-2}]$	$\alpha_p [cm^{-2}]$
A	$2.0 \cdot 10^{-10}$	$1 \cdot 10^{-18}$	$2 \cdot 10^{-18}$
B	$2.0 \cdot 10^{-10}$	$5 \cdot 10^{-17}$	$1 \cdot 10^{-18}$
C	$2.0 \cdot 10^{-10}$	$1.5 \cdot 10^{-18}$	$3 \cdot 10^{-18}$
D	$1.0 \cdot 10^{-10}$	$1.5 \cdot 10^{-18}$	$3 \cdot 10^{-18}$
E	0	$1.5 \cdot 10^{-18}$	$3 \cdot 10^{-18}$
F	0	$1.5 \cdot 10^{-18}$	$3 \cdot 10^{-18}$

factor in *Physics* section of Synopsys command file. An agreement between experiment and calculation is reached for A_{ph} of about 0.059. This low value of A_{ph} should not be surprising. If carrier drift-diffusion processes only were responsible for transport than A_{ph} close to 1 would be expected. However, we are dealing here, in particular in waveguide and in QW regions, with ballistic transport as well, while the computational model used in Synopsys is derived from drift-diffusion equations, modified for dealing with transport through QW as discussed in the next section.

Other parameters available in Synopsys, important in this case, are these related to light absorption and carrier scattering. Experiment shows that absorption coefficient is of the order of $1cm^{-1}$ ([3]). It is argued that in AlGaAs lasers the main contribution to absorption is due to scattering on free carriers. The free carrier absorption coefficient, α_{fc} , is given by:

$$\alpha_{fc} = (\alpha_n \cdot n + \alpha_p \cdot p) \cdot L, \quad (1)$$

where n and p are the electron and hole density, and L is light intensity. We choosed in our calculations such values of α_n and α_p that an effective absorption coefficient would be obtained close to that experimental one.

It is important also to have a reasonable value of radiative recombination rate, R_r , which is assumed to be described by:

$$R_r = C \cdot \left(n \cdot p - n_{i_{eff}}^2 \right), \quad (2)$$

where $n_{i_{eff}}$ describe the effective intrinsic density, and C is a parameter available for changes.

Typical $I-V$ characteristics computed at $T = 300$ are shown in Figure 1, for a broad range of QW widths. For current near the lasing threshold current I_{th} (i.e. for voltage near the lasing offset voltage U_0), which correspond to a kink in $I-V$, for most of these curves the results are very well approximated by a phenomenological modified exponential relation ([7]):

$$\begin{aligned} I(U) &= I_{th} \cdot \exp(A \cdot (U - U_0) + B \cdot (U - U_0)^2), \quad \text{for } U < U_0 \\ I(U) &= I_{th} \cdot \exp(C \cdot (U - U_0) + D \cdot (U - U_0)^2), \quad \text{for } U > U_0 \end{aligned} \quad (3)$$

where I_{th} , U_0 , as well A , B , C , and D are certain fitting parameters.

There is no simple, straightforward interpretation of these curves above the lasing threshold, where a strong interplay between the effects of carrier transport and scattering takes place, with light absorption as well. However, we may notice an interesting feature for parts of curves below the lasing threshold. While the width of QW, d_a , changes (nearly) monotonically, the curves however are grouped into a few sets such that they nearly coincide together within each group.

A very similar feature is observed when gain or loss is drawn as a function of current, for many widths of active region (Figure 3). Again, we see that datacurves for current below the lasing threshold (that corresponds to kinks in curves) are grouped into a few sets such that they nearly coincide together within each group. If gain or loss were drawn as a function of voltage, however, we would not see such a grouping.

Therefore, we conclude that below the lasing threshold, current as a function of QW width at constant voltage derived from the data like these in Fig.

1, or gain or loss as a function of QW width, at constant current values, also below the lasing threshold, will follow step-like functions.

This is illustrated in Fig. 2, where current as a function of QW width derived at constant voltage from datacurves similar to these as in Figure 1 is shown. Figure 2 presents data computed at different conditions, and marked from A to F , for several combinations of free carrier scattering coefficients, α_n and α_p , and values of C , the radiative recombination parameter, as described in Table 1. Moreover, dataset F differs from datasets A - E . The last are computed assuming changing Al concentration in waveguides (when Al in QW is kept constant) in such a way that the lasing wavelength does not change with the change of QW width. The dataset F is computed for constant Al concentration in waveguides of 33%. The solid line in Fig. 2 is drawn through datapoints F , and arrows there refer to curve F as well, and indicate positions of bound QW energy states crossing the conduction- or valance band offset energies. Positions of bound QW energy states for cases A - E , as illustrated in Fig. 5, are very close to but not identical.

The step-like features are preserved also in $I_{th}(d_a)$ dependencies, as illustrated in Fig. 4. There, however, effects of carrier scattering and light absorption smear-out the picture. It is useful to notice that at some values of QW width no lasing action is reached, and therefore the datapoints in that Figure are not available for all QW widths.

Changes of QW height (caused by difference of Al concentration in QW and waveguides) cause very similar step-like dependencies. Moreover, the effects are in some situations more clear and pronounced at low temperatures. We did modelling for $T=77.6$ K to confirm their existence.

Moreover, with a careful design of laser structure (content of Al in QW and waveguides) it is possible to find the evidence of the effect in temperature dependence of current, when measurements are performed at constant voltage. Energy gap in active region, as well energy gap in waiveguides change in a nearly the same way when temperature changes, but not in exactly the same way. We found such Al concentrations when the number of QW bound states changes with temperature swap. Figure 6 shows how the uppermost bound electron state energy, E_4 in this case, differs from E_{CBO} (energy levels of other QW bound states do not play a significant role in this case), for a three Al concentrations in waveguide, when Al concentration in QW is 8%. For Al concentration 34.70%, the E_4 energy level exists always through temperature swap studied. For Al concentration 34.65%, the E_4 energy level does not exist between around 150 and 370K. For Al concentration 34.60%, it exists at temperatures higher than about 470K, only. This has profound

implications on $I(T)$ dependencies measured at constant voltage for these three different Al concentrations of Al in waveguide, as Figure 7 illustrates. For 34.60% and 34.70% of Al content, we observe continuous $I(T)$ curves. However, for 34.65% of Al content, at low temperatures $I(T)$ results fall on curve that has been computed for 34.60% of Al, and at high temperatures they fall on the curve computed for 34.70% of Al.

3 Discussion

In case of tunneling energy barrier, transfer matrix approach is used to describe charge transport through it ([5], [6]). The interband tunneling current is written as

$$J \sim \int_{E_{min}}^{E_{max}} N(E) \cdot f(E) \cdot T(E) \cdot dE \quad (4)$$

where $T(E)$ is energy-dependent tunneling rate, $N(E)$ is the density of states, $f(E)$ is the Fermi-Dirac distribution function, respectively, and E_{min} and E_{max} are minimum and maximum carrier energies available.

In Sentaurus, the following intuitive model is used to handle the physics of carrier scattering at the quantum well (Figure 8). The carrier populations are separated into bound and continuum states, and separate continuity equations are applied to both populations. The QW scattering model accounts for the net capture rate, that is, not all of the carriers will be scattered into the bound states of the quantum well. The electron capture rate from the continuum (subscript C) to the bound (subscript B) states is:

$$R = \int_{E_c}^{\infty} dE_C \int_{E_w}^{\infty} dE_B \cdot N_C(E_C) \cdot N_B(E_B) \cdot S(E_B, E_C) \cdot f_C(E_C)(1 - f_B(E_B)) \quad (5)$$

where E_c and E_w is energy of lowest conduction band-, and bound QW electron states, $N(E)$ is the density-of-states, $S(E_B, E_C)$ is the scattering probability, and $f(E)$ is the Fermi-Dirac distribution. The reverse process gives the electron emission rate from the bound to continuum states:

$$M = \int_{E_c}^{\infty} dE_C \int_{E_w}^{\infty} dE_B \cdot N_C(E_C) \cdot N_B(E_B) \cdot S(E_B, E_C) \cdot f_B(E_B)(1 - f_C(E_C)) \quad (6)$$

The net capture rate is $C = R - M$, and for very deep quantum wells (keyword *QWDeep* must be used for that in Sentaurus) is known to be given by approximation:

$$C = R - M = (1 - \exp(\eta_B - \eta_C)) \cdot \frac{n_C}{\tau} \quad (7)$$

where $\eta_B = (-q\Phi_B - E_C)/k_B T$ and $\eta_C = (-q\Phi_C - E_C)/k_B T$ contain the quasi-Fermi level information and τ is the capture time. The capture time represents scattering processes attributed to carrier-carrier and carrier-LO phonon interactions involving bound quantum well states. The net capture rate C is added to the continuity equations as a recombination term.

In a similar way scattering of holes is computed, with their own characteristic capture time. These parameters are specified in Sentaurus by the keywords *QW eScatTime* and *QW hScatTime*. Their default values, $8 \cdot 10^{-13} s$ and $4 \cdot 10^{-13} s$, respectively, correspond reasonably well to these based on theory ([8], [9]). Photoluminescence spectroscopy results give values of an order of $3 - 20 ps$ [9]. In most of our modelling, if not indicated otherwise, we use also default values of electron and hole mobility, represented in Sentaurus by parameters $eQW Mobility = 9200 cm^2/Vs$ and $hQW Mobility = 400 cm^2/Vs$.

For shallow quantum wells, the energy transfer during scattering can only occur in a limited range. In the limit of elastic scattering, the net capture rate is then approximated by:

$$C = \left(\frac{F_{3/2}(\eta_C)}{F_{1/2}(\eta_C)} - \frac{F_{3/2}(\eta_B)}{F_{1/2}(\eta_B)} \right) \cdot \frac{n_C}{\tau} \quad (8)$$

where F_m is the Complete Fermi-Dirac integral of the order of m . The shallow quantum well model is activated by the keyword *QWShallow*.

It should be pointed out that Equations 7 and 8, for deep and shallow quantum wells, respectively, while provide a convenient, intuitive description of carriers scattering and capture on QW, these are approximate only. In particular, there is no dependence of capture time on energy of unbound carriers there and no periodic oscillations as a function of QW size ([8], [9]). GaAs/AlGaAs are considered to have deep quantum wells. However, as we

have shown, the results of our modelling indicate on a strong role of bound QW states located very closely to the offset energy levels of quantum wells. For these reasons, we did not restrict our calculations to deep- or shallow-QW models but used instead the full model available in Sentaurus.

Equations 4 - 6 all depend on density of bound states in QW. We expect hence that current through the QW will be proportional to the density of all bound states in QW. In effective mass approximation, the two-dimensional density of electron states within each QW subband n equals ([6])

$$N_n(E) = \frac{m_n}{\pi\hbar^2}, \quad \text{for } E > E_n \quad (9)$$

Hence, the current should be proportional to the *number of bound states* \times *carrier mass*. The quantity computed this way (with a certain multiplication factor) is represented by large circles in Figure 2. Though it must not be exact (for instance, no difference in scattering rates for electrons and holes is accounted for), it fits reasonably well $I(d_a)$ dependence.

4 Summary and Conclusion

When performing modeling of laser characteristics as a function of the width of active region we noticed a non-monotonic, discontinuous dependence of $I(d_a)$ (when measured at constant voltage applied). A careful analysis of the data led us to the hypothesis that discontinuities occur when the most upper QW, bound energy states are found very close to the conduction or valence band energy offsets. The effect, hence, is thought to be related to changes in density of states of carriers from one hand, and to fast changes in carrier transfer matrix through QW for QW bound states close to E_{CBO} or E_{VBO} . As such, it ought to be more pronounced at lower temperatures. Indeed, results of modeling $I(d_a)$ at liquid Nitrogen temperature (77.6 K) confirmed this idea.

The effect is observed also when modelling current as a function of QW depth (Al concentration in waveguide).

Therefore, we concluded that a similar effect will be present also in modelling I as a function of temperature. In that case however a careful design of laser properties is needed, in such a way that a transition of the most upper QW energy state will pass through an edge of quantum well when temperature is swapt.

These observations are important for proper designing of semiconducting lasers (choice of Al concentrations, thickness of the active region, etc). However, they also illustrate well the intrinsic carrier transport mechanisms in SCH lasers. Potentially, might be useful as a kind of quantum level spectroscopy tool when testing laser designs for technological applications.

References

- [1] *Sentaurus TCAD User Guide*, Synopsys, 2010, www.synopsys.com
- [2] C. W. J. Beenakker and H. van Houten, *Quantum Transport in Semiconductor Nanostructures*, Solid State Physics, 44, 1-228 (1991)
- [3] A.V. Andreev, A.Y. Leshko, A.V. Lyutetskiy, A.A. Marmalyuk, T.A. Nalyot, A.A. Padalitsa, N.A. Pikhtin, D.R. Sabitov, V.A. Simakov, S.O. Slipchenko, M.A. Khomylev, I.S. Tarasov, *High power laser diodes ($\lambda = 808 - 850$ nm) based on asymmetric separate confinement heterostructure*, Semiconductors, 2006 40(5), 628-632.
- [4] A.Yu. Andreev, S.A. Zorina, A.Yu. Leshko, A.V. Lyutetskiy, A.A. Marmalyuk, A.V. Murashova, T.A. Nalet, A.A. Padalitsa, N.A. Pikhtin, D.R. Sabitov, V.A. Simakov, S.O. Slipchenko, K.Yu. Telegin, V.V. Shamakhov, I.S. Tarasov, *High power lasers ($\lambda = 808$ nm) based on separate confinement AlGaAs/GaAs heterostructures*, Semiconductors, 2009, 43(4), 543-547.
- [5] John H. Davies, *The Physics Of Low-Dimensional Semiconductors. An Introduction*, Cambridge University Press, 1998.
- [6] Joachim Piprek, *Semiconductor Optoelectronic Devices. Introduction to Physics and Simulation*, Academic Press, 2003.
- [7] Zbigniew Koziol, and Sergey I. Matyukhin, *Modified exponential $I(U)$ dependence and optical efficiency of AlGaAs SCH lasers in computer modeling with Synopsys TCAD*, arXiv:1107.4668v1 [cond-mat.mtrl-sci] (2011).
- [8] J. Hernández-Rosas, L. Villegas-Lelovsky and G. González de la Cruz, *Capture of carriers by quantum wells via optical-phonon deformation potential*, Revista Mexicana de Física 48 (4) 295–299, 2002.
- [9] P. W. M. Blom, C. Smith, J. E. M. Haverkort, and J. H. Wolter, *Carrier capture into a semiconductor quantum well*, Phys. Rev. B 47, 2072, 1993.

- [10] Jong-Jae Kim, Woo-Pyo Hong, and Seoung-Hwan Park, *Well-Width Dependence of the Threshold Current Density of Type-II GaAsSb/GaAs Quantum Well Lasers*, Journal of the Korean Physical Society, 48, p. 166, 2006.

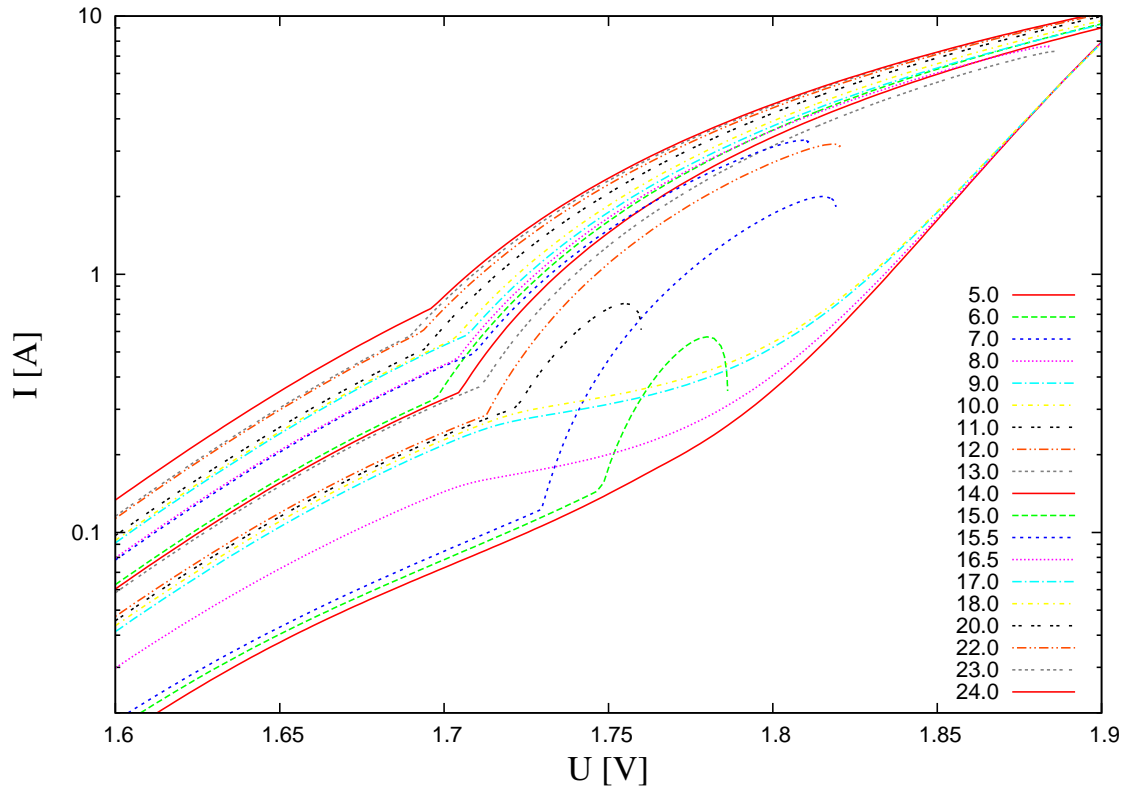


Figure 1: Typical $I - V$ characteristics computed at $T = 300$. *OpticalLoss* parameter is assumed 0, no radiative recombination, free carrier scattering rate parameters τ_n and τ_p are $8 \cdot 10^{-13} s^{-1}$ and $4 \cdot 10^{-13} s^{-1}$, with electron and hole mobilities $9200 cm^2/Vs$ and $400 cm^2/Vs$. The legend describes width of QW (in nm), from $5nm$ from right-bottom curve to $24nm$ for uppermost curve.

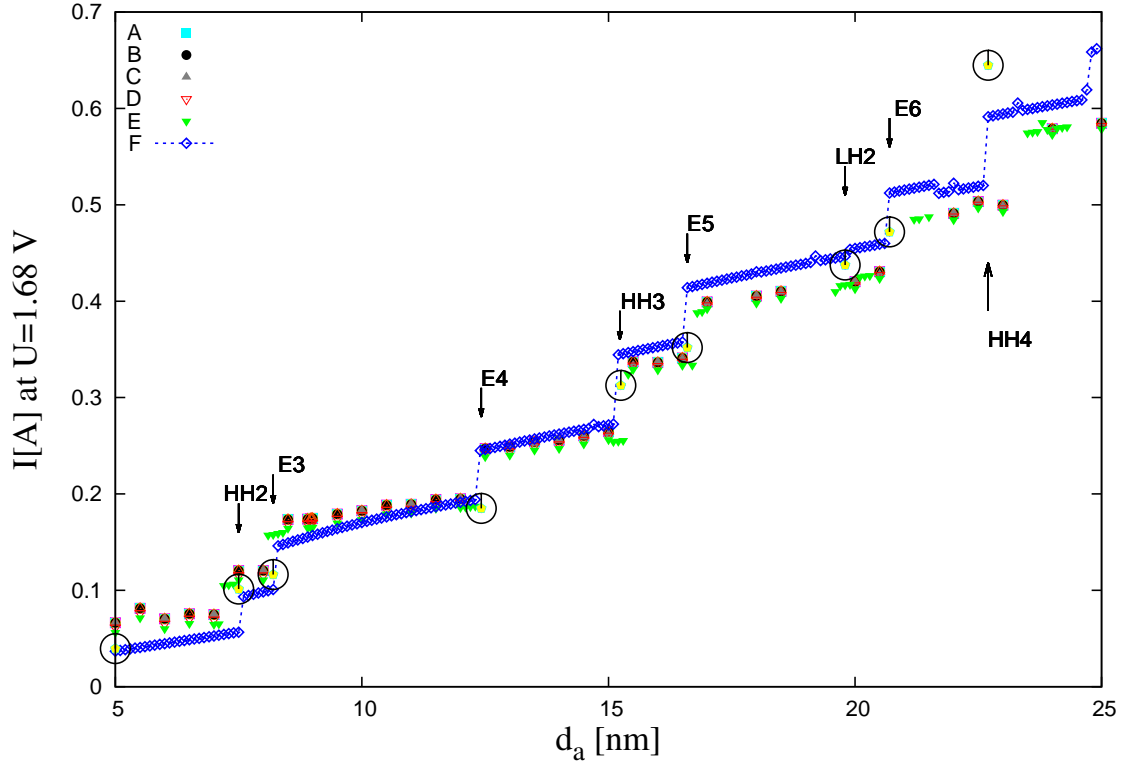


Figure 2: Current as a function of QW width derived at constant voltage from datacurves as these shown in Figure 1 and described in Table 1. The solid line for datapoints F is to guide the eyes, only. F is computed for constant Al concentration in QW of 8%, while all other datasets ($A - E$) are computed with such a concentration of Al in QW that lasing wavelength will remain constant ($808nm$) when QW width changes. The arrows are for datapoints F .

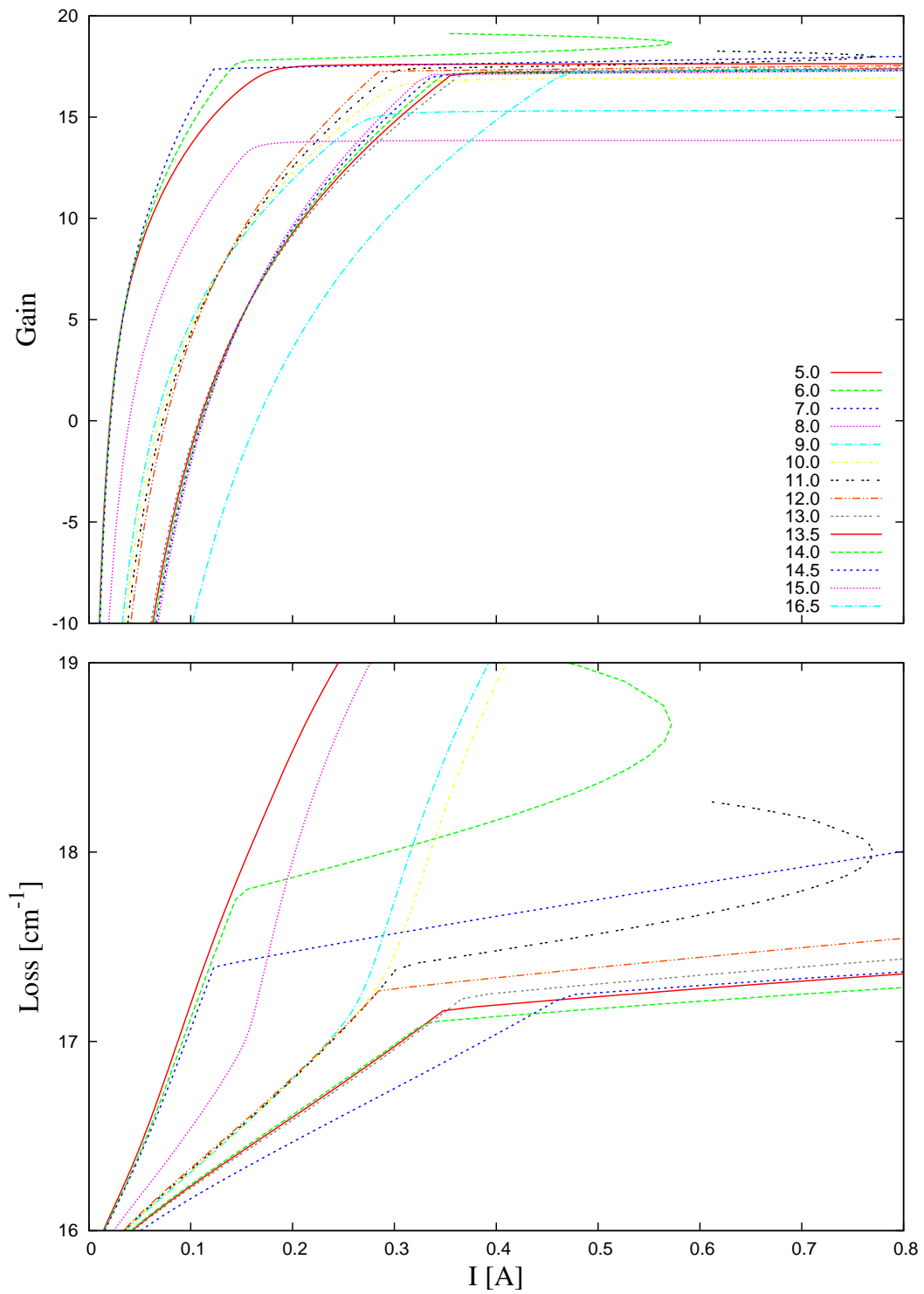


Figure 3: Gain (upper figure) and loss computed for in similar conditions as the data in Figure 1. The legend describes width of QW (in nm).

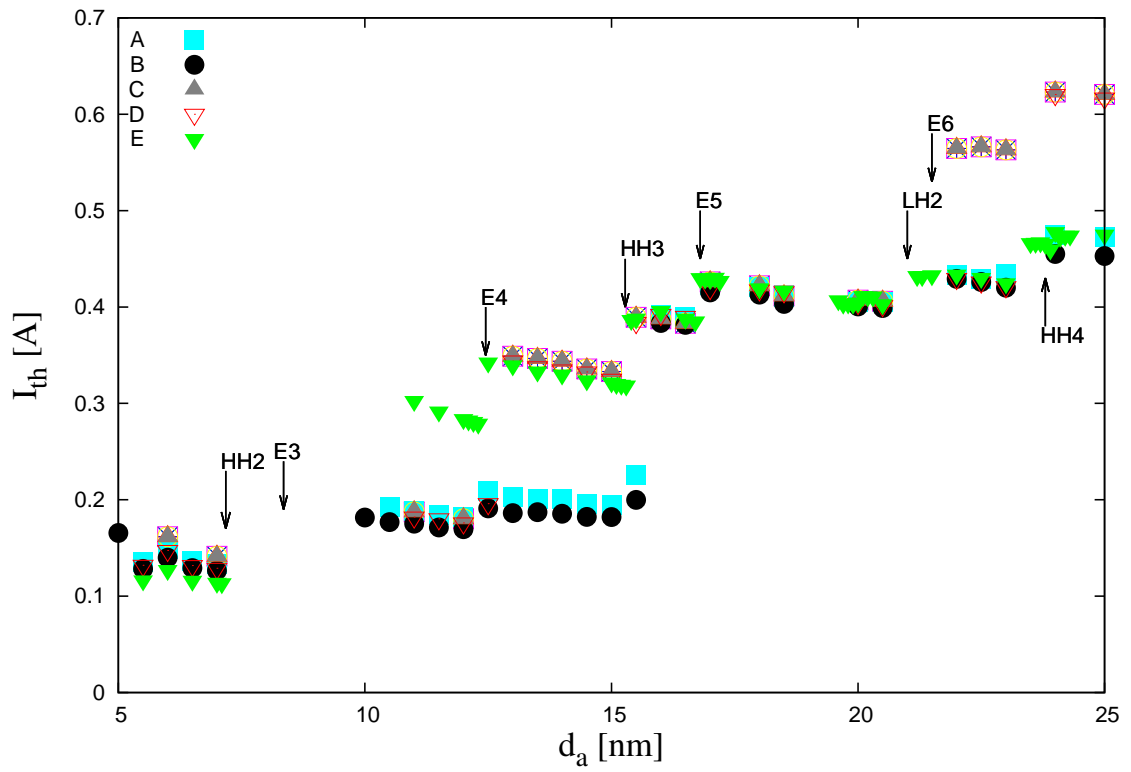


Figure 4: Lasing threshold current as a function of QW width for datasets as these shown in Figure 1 and described in Table 1. The arrows are at positions close to but not identical to these in Figure 2.

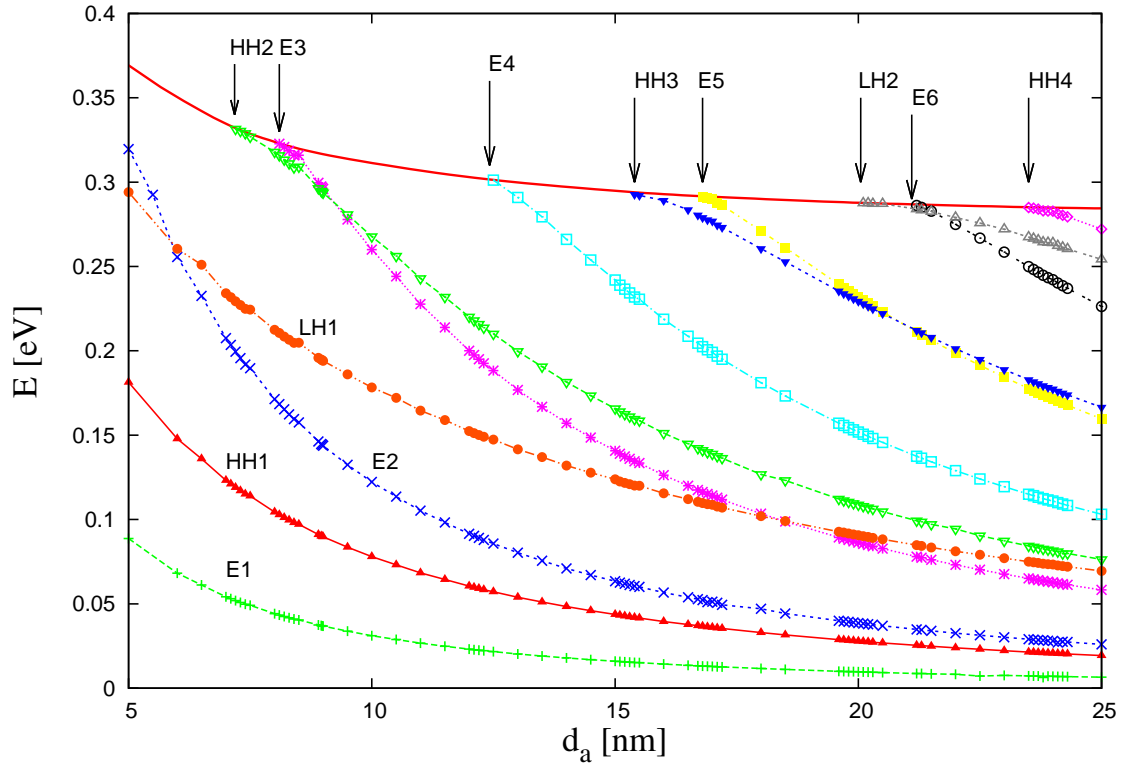


Figure 5: $T=300\text{K}$. Conduction and valence band offset energy, (E_{CBO} and E_{VBO}), and electron (E_n), light- and heavy hole energies (LH_n and HH_n) in QW, as a function of QW width. Hole energies and E_{VBO} have been scaled up by a factor 28 to obtain coincidence with electron energy scale (E_{CBO} and E_{VBO} curve are the same in this Figure).

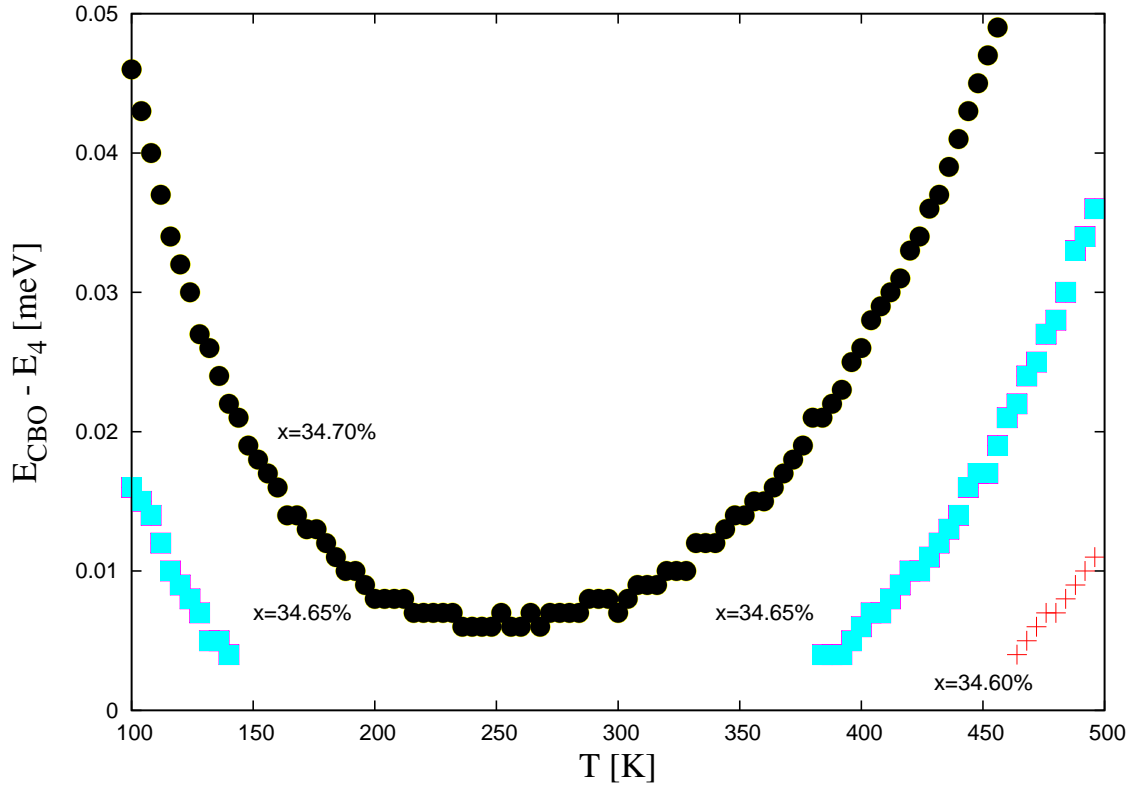


Figure 6: The energy difference between conduction band offset energy E_{CBO} and the closest to it bound electron state in QW, E_4 , as a function of temperature, when active region concentration is 8% of Al, for three values of waveguide Al concentration: 34.60%, 34.65%, and 34.70%.

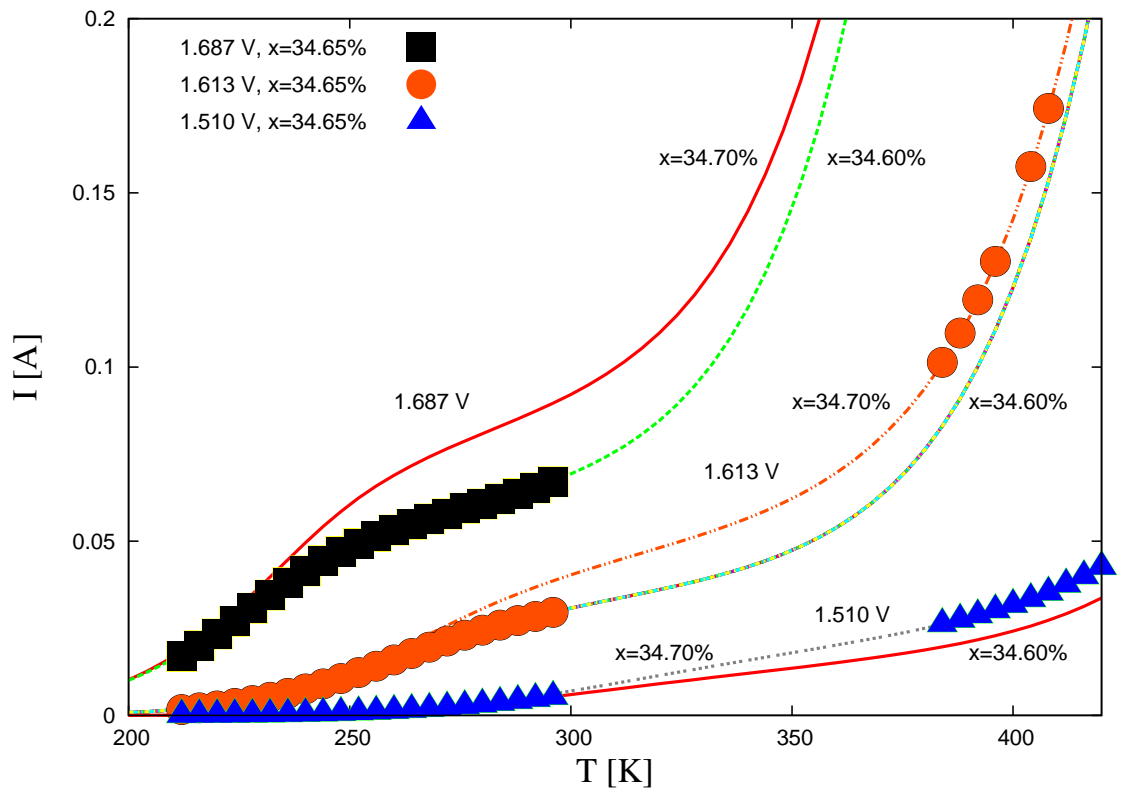


Figure 7: Temperature dependence of current for free values of voltage applied (1.510V, 1.613V, and 1.687V; for each of these this is below the lasing threshold), and for free values of Al concentrations in waveguide, the same as in Figure 6.

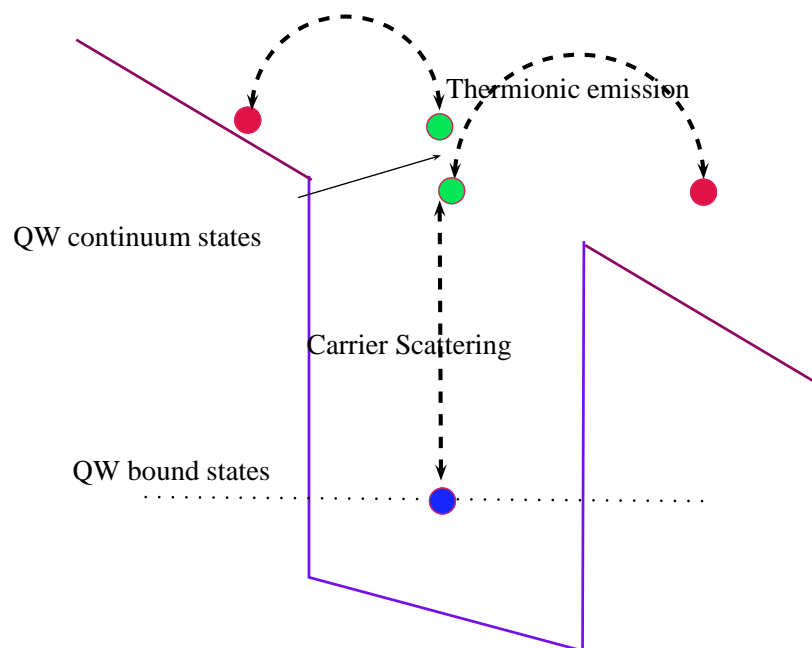


Figure 8: The model of carrier scattering at the quantum well used in Sentaurus (based on [1]).